HHS Public Access

Author manuscript

Biochem Pharmacol. Author manuscript; available in PMC 2020 January 01.

Published in final edited form as:

Biochem Pharmacol. 2019 January ; 159: 64–73. doi:10.1016/j.bcp.2018.11.008.

Serine residues in the α4 nicotinic acetylcholine receptor subunit regulate surface α4β2* receptor expression and clustering

Cristian A. Zambrano[1], **Daniela Escobar**[1], **Tania Ramos-Santiago**[1], **Ian Bollinger**[1], **Jerry Stitzel**[1,2]

[1]Institute for Behavioral Genetics, University of Colorado Boulder, USA

[2]Department of Integrative Physiology, University of Colorado Boulder, USA

Abstract

Background and purpose: Chronic nicotine exposure upregulates α4β2* nicotinic acetylcholine receptors (nAChRs) in the brain. The goal of this study was to examine the role of three serine residues in the large cytoplasmic loop of the α4 subunit on α4β2* upregulation in neurons.

Experimental approach: Serine residues S336, S470 and S530 in mouse α4 were mutated to alanine and then re-expressed in primary neurons from cortex, hippocampus and subcortex of α4 KO mice. Mutant and wild type α4 expressing neurons were treated with nicotine (0.1, 1 and 10 μM) and assessed for α4β2* upregulation.

Key results: α4β2* nAChRs expressing S336A or S470A mutants were deficient at cell surface upregulation in both subcortex and hippocampal neurons. S530A α4β2* mutants exhibited aberrant surface upregulation in subcortical neurons. None of the mutants affected surface upregulation in cortical neurons or upregulation of total α4β2* binding sites in any region. Further, dense domains or clusters of α4β2* nAChRs were observed in the neuronal surface. The impact of nicotine exposure on the intensity, area, and density of these clusters was dependent upon individual mutations.

Conclusions and implications: Effects of α4 nAChR mutants on surface upregulation varied among brain regions, suggesting that the cellular mechanism of α4β2* upregulation is complex and involves cellular identity. We also report for the first time that α4β2* nAChRs form clusters on the neuronal surface and that nicotine treatment alters the characteristics of the clusters in an α4 mutant-dependent manner. This finding adds a previously unknown layer of complexity to the effects of nicotine on α4β2* expression and function.

Conflict of interests: none.

Keywords

nAChR; upregulation; nicotine; clusters; [^{125}I]epibatidine

1. Introduction:

nAChRs are ligand gated ion channels expressed in the nervous system and in some non-neuronal cells. Although acetylcholine (ACh) is the endogenous ligand for these receptors, nicotine and other natural and synthetic compounds also activate these receptors. Sixteen distinct subunits are found in mammals (α1–α7, α9-α10, β1–β4, γ, δ, ε). Theoretically, many different subunit combinations are possible, however, only a fraction of the possible receptor subtypes are known to exist. In brain, the heteromeric α4β2* (the asterisk denotes the possible inclusion of other subunits) is the most abundant nAChR and this nAChR subtype has been implicated in nicotine self-administration, reward, and dependence, and in diseases such as Alzheimer's and epilepsy [1]. Paradoxically, chronic nicotine exposure in humans, animal models and in vitro culture systems increases the expression of α4β2* nAChRs [2–8]. This increase, or upregulation, is thought to compensate for functional desensitization observed after prolonged nicotine exposure. Several mechanisms of nicotine-mediated up-regulation have been proposed and include, but are not limited to, nicotine-dependent changes in the rate of nAChR turnover [9,10] and nicotine serving as a molecular chaperone [11,12]. However, it is important to note that whatever the mechanism of up-regulation, it must account for the fact that nAChR up-regulation is brain region dependent. Substantial up-regulation of α4β2* nAChRs is readily observed in regions including the cerebral cortex and hippocampus but in other regions upregulation is less robust or absent [2,13–16]. This brain region specific up-regulation to chronic nicotine is replicable in primary neuronal cultures [7,8].

The large intracellular loop between transmembrane domains 3 (MIII) and 4 (MIV) of the α4 nAChR subunit is thought to be involved in the regulation of nAChR assembly, trafficking and function [17]. One amino acid in the MIII-MIV loop that has been shown to be critical for nicotine-induced upregulation of α4β2 nAChRs in frog oocytes is a serine at residue S336 in the rodent α4 subunit (S334 in human α4) [18]. However, it has not been determined whether S336 is critical for upregulation in neurons or whether its role in upregulation is dependent upon neuronal cell type. The second site of interest is a serine residue at position S470 in the mouse α4 subunit (S467 in human α4). S470 modulates trafficking of α4β2 nAChRs to the cell surface in HEK293 cells through an interaction with the chaperone 14–3-3η [19–21]. The role of this amino acid in nicotine-induced upregulation is unknown.

To determine the role of the S334 and S470 in nicotine-mediated upregulation in neurons, α4β2* nAChR binding sites were established by infection of primary neurons prepared from α4 KO mice with adeno associated virus (AAV) containing cDNAs for WT α4 nAChR subunit or α4 nAChR with the point mutation S336A or S470A. A third serine within the MIII-MIV loop, S530, also was examined. The selection of the S530 site is based on unpublished data from our laboratory that indicates that mutating this site substantially

increases α4β2 function in transfected HEK293T cells. Primary neurons were derived from three brain areas: the cortex (Cx), hippocampus (Hp) and subcortex (diencephalon and hindbrain, SCx) to assess whether any effects of the mutants were brain-region selective. Following vehicle or nicotine treatment of the infected neurons, differential [^{125}I]epibatidine binding was performed to assess total, intracellular and surface expression of α4β2* nAChRs and immunocytochemistry was conducted to explore the potential impact of nicotine exposure and/or the mutant α4 subunits on the surface distribution of α4β2 nAChRs.

2. Materials and Methods:

2.1. Materials

Neurobasal media, Minimal essential media (MEM), B27 supplement, GlutamaxTM, inactivated horse serum and TrypLE express (trypsin solution) were purchased from Invitrogen (Carlsbad, CA). [^{125}I]epibatidine (2200 Ci/mmol) was purchased from Perkin-Elmer Life Science (Waltham, MA). 2-(2-bromoacetyloxy)-N,N,N-trimethylethanaminium bromide (BrACh), cytisine, cytosine β-D-arabino-furanoside (ARA C), 5,5'-dithio-bis(2-nitrobenzoic acid (DTNB), 1,4-dithio-DL-treithol (DTT), (−)-nicotine hydrogen tartrate, polyethyleneimine (PEI), and poly-l-lysine (> 30,000 kDa) were purchased from Sigma Aldrich Chemical Company (St. Louis, MO). 4-(2-Hydroxyethyl)-piperazineethanesulfonic acid (HEPES) half-sodium salt was from Roche Diagnostics Corporation (Indianapolis, IN).

2.2. Site-directed mutagenesis and AAV production

A triple hemagglutinin (HA) tag was introduced to the c-terminal end of the mouse α4 nAChR cDNA as follows: A triple HA tag sequence from plasmid pKH3 (Addgene Plasmid #12555) was inserted in frame to the c-terminus of the mouse α4 nAChR sequence. The α4-HA sequence was then sub cloned in a pAAV-hSyn-WPR plasmid (kindly donated by Dr. Charles Hoeffer, University of Colorado). Serine to alanine site directed mutagenesis was performed to target serines 336, 470 and 530 of the nascent mouse α4subunit sequence. Multiple clones for each mutation were sequenced in their entirely to ensure that the mutagenesis introduced the desired mutation but not any other mutations. The AAV vector with the α4 WT, S336A, S470A and S530A mutations were packaged into AAV serotype 2 (AAV2) virus by the University of Pennsylvania Vector Core (Philadelphia, PA).

2.3. Primary neuronal culture

All procedures involving the use of live animals were approved by the IACUC of the University of Colorado and conform to the guidelines for animal care and use set by the NIH and the Guide for the Care and Use of Laboratory Animals (8th Ed.). Primary cultures from C57BL/6J or α4 KO (previously characterized, Ross et al., 2000) embryonic mouse brains (embryonic day E16-E18) were prepared as previously described [22]. Embryo brains were placed in Hank's balanced salt solution (HBSS) (Ca^{2+} and Mg^{2+} free) buffer and separated from the meninges. Cerebral cortex was dissociated from brain stem, the hippocampus was dissected from the cortex, and the remaining tissue represents subcortex (diencephalon, midbrain and hindbrain). Brain tissues were minced into small pieces, rinsed once with HBSS and then incubated for 15 min. at 37°C with 0.5X TrypLE express diluted with

HBSS. TripLE solution was replaced by minimal essential medium (MEM) supplemented with 10% Horse Serum and mechanically disaggregated through a heat polished Pasteur pipette. The cell suspension was centrifuged at 800 × g for 2 minutes and then re-suspended in MEM 10% Horse Serum, 100 U/ml penicillin, 100 U/ml streptomycin, and 0.25 mg/ml amphotericin B. Isolated neurons were seeded at a density of 100,000 cells/cm^2 over polystyrene plates coated with 0.1 mg/ml poly-l-lysine prepared in 0.1 M borate buffer pH 8.5. After 24 hours, media was changed to maintenance media (neurobasal media supplemented with B27, 100 U/ml penicillin, 100 U/ml streptomycin, 0.25 mg/ml amphotericin B and 2 mM L-glutamine. On the second day of culture, 10 μM ARA C was added for 48 hours to control proliferation of glial cells. Cultures were kept in a humidified 5% CO_2-95% air incubator at 37°C. Stock solutions of nicotine free base (10 mM) were prepared in maintenance media and kept frozen at −20°C until used. Neurons were cultured in 12-well plates (3.8 cm^2 surface area per well) for binding assays or 12 mm diameter glass coverslips inserted in 24-wells plates (1.9 cm^2 surface area per well) for immunofluorescent studies. Infection with AAVs containing wild type or S336A, S470A, S530A mutations were performed at day in vitro 4 (DIV4). Titers were set at 3.3×10^9 GC for a cell density of 100,000 cells/cm^2. Ten days after viral infections, neurons were challenged with 0.1, 1 or 10 μM nicotine tartrate up to 4 days. These nicotine concentrations previously have been shown to produce concentration-dependent α4β2* nAChR upregulation in primary neuronal cultures [7,8,22,23].

2.4. Preparation of total membranes

Neurons were rinsed once with Krebs-Ringer-HEPES (KRH) buffer (NaCl, 144 mM; KCl, 2.2 mM; $CaCl_2$, 2 mM; $MgSO_4$, 1 mM; HEPES, 25 mM; pH = 7.4) and then lysed in 10 times diluted KRH buffer (hypotonic KRH buffer). Cell lysates were collected from the cell culture dish and centrifuged at 25,000 × g for 10 min at 4°C. Pellets were washed 3 times by resuspension in ice-cold hypotonic KRH buffer followed by centrifugation. Cell membrane pellets were resuspended in distilled-deionized water for the binding reaction (if carried out immediately) or in hypotonic 0.1X KRH binding buffer and frozen at −20 °C until assayed.

2.5. [^{125}I]epibatidine binding to cell membrane homogenates

[^{125}I]Epibatidine binding was measured as described previously [8]. Frozen cell membrane pellets were thawed and centrifuged at 25,000 × g for 10 min. The supernatant was discarded, and the pellet was resuspended in deionized-distilled water. Resuspension volumes varied among samples to adjust protein concentrations such that less than 10% of the [^{125}I]epibatidine was bound to the protein at a concentration of 200 pM of the radioligand. Samples (5–20 μg protein) were incubated in 96-well polystyrene plates for 2 hours at room temperature in KRH buffer with a final incubation volume of 30 μl. At the completion of the binding reaction, samples were diluted with 200 μl of ice-cold KRH buffer and filtered under vacuum (0.2 atm.) onto glass fiber filters that had been treated for 10 minutes with 0.5% polyethelenimine (top filter, MFS Type B; bottom filter, Gelman A/E). An Inotech Cell Harvester (Inotech Biosystems International, Rockville, MD) was used to collect the samples, which were subsequently washed five times with ice-cold buffer. Filters containing the washed samples were transferred to glass culture tubes and radioactivity counted at 80% efficiency using a Packard Cobra Auto-Gamma Counter (Packard

Instruments, Downers Grove, IL). For all the experiments, nonspecific binding was measured by including 100 μM cytisine in the incubation medium. Since [^{125}I]epibatidine binds with high affinity to several different nAChR subtypes control neurons that had not been infected with any of the AAVs were used to determine basal non-α4β2* binding sites.

2.6. Alkylation of plasma membrane associated nAChR

Alkylation of surface nAChR was done as described before [8]. Briefly, primary neurons in culture were rinsed once with HBSS buffer pH 7.4 (HBSS) supplemented with 20 mM HEPES and then treated for 15 min at 37 °C with 1 mM DTT prepared in HBSS to reduce disulfide bonds. Cultures were rinsed once with HBSS followed by 6 min. incubation at room temperature with 100 μM BrACh, a cholinergic ligand that is not cell permeant, prepared in HBSS. After rinsing with HBSS, reduced disulfide groups were re-oxidized by adding 1 mM DTNB in HBSS for 15 min at 37°C. After the alkylation reaction, the neurons were rinsed once with HBSS, lysed with hypotonic ice-cold KRH buffer and scraped from the plate. A set of cultures treated as described above, but omitting the BrACh incubation, was used to measure total [^{125}I]epibatidine binding. Whole particulate membranes were prepared as described above and [^{125}I]epibatidine binding was subsequently measured using the radioligand binding assay described above in [^{125}I]epibatidine binding in cell membrane homogenates. Surface binding was calculated as the difference between total binding (no incubation with BrACh) and binding after alkylation (intracellular).

2.7. Intracranial AAV injections

Adult C57/BL6J mice (45–60 days old) were anesthetized with 80 mg/kg Ketamine, 8 mg/kg Xylazine and 1 mg/kg Acepromazine cocktail and then secured in the stereotaxic apparatus. Buprenorphine (1 mg/kg) was administered to induce analgesia. The scalp was shaved and cleaned with Iodine. A small midline incision of approximately 1 cm was made in the scalp to expose the dorsal surface of the skull. Tissue was dissected, and bone cleared with rubbing alcohol. Bregma and Lambda were set to the equal dorsoventral distance. Two bilateral injection sites were drilled through the calvaria with a micro drill bit at site 1: +/ −1.8 lateral, −2.1 anteroposterior, 1.6 dorsoventral and site 2: +/− 2.5 lateral, −2.8 anteroposterior, 2.1 dorsoventral. These injection sites targeted the dentate gyrus of the dorsal hippocampus. A volume of 75 nl of AAV (4×10^{12} GC/ml) was injected at a rate of 7.5 nl/min. After confirming there was not bleeding at the injection site, the scalp was glued using Vetbond glue (3M™). Mice were place in a thermoregulated mat until recover from anesthesia.

2.8. Preparation of coronal brain sections

Mice were sacrificed by cervical dislocation. the brains were removed from the skulls and rapidly frozen by immersion in isopentane (−20 °C, 10 s). The frozen brains were wrapped in aluminum foil, packed in ice, and stored at −70 °C until sectioning. Tissue sections 14 μm thick prepared using a Leica Model 1850 cryostat refrigerated to −16 °C were thaw-mounted onto Superfrost®/plus microscope slides (Fisher Scientific). Mounted sections were stored, desiccated, at −70 °C until use. Ten series of sections were collected from each mouse brain.

2.9. Immunofluorescence

Detection of α4β2* nAChR expressed in the plasma membrane was done in wild type C57BL/6J neurons expressing native α4β2* nAChR, α4 KO neurons infected with AAVs containing WT and S336A, S470A and S530A mutations and coronal brain sections of α4 KO mice intracranially injected with WT α4 subunit AAV. Neurons post-treatment and coronal brain sections were fixed with 4% PFA for 15 minutes at 37°C. Five minutes incubation with 0.2% TRITON X100 was necessary to detect surface and intracellular receptors, however this step was skipped if only surface receptors were stained. Nonspecific sites were blocked with 5% BSA overnight at 4°C. For α4 KO neurons infected with AAVs, α4β2* receptors were stained with anti HA antibody (rabbit anti HA-probe Y-11, Santa Cruz Biotechnology, Dallas TX, USA) followed by CY3 conjugated secondary antibody (donkey anti-rabbit-CY3, AP182C, Sigma-Aldrich, St. Louis, MO, USA). Native α4β2* nAChR were detected with both, monoclonal antibody 299 (rat mAb299, ABCAM, Cambridge, UK) which binds to α4 subunits followed by TRITC conjugated secondary antibody (donkey anti rat-TRITC, T4280, Sigma-Aldrich, St. Louis, MO, USA) and with anti β2 antibody (rabbit anti β2, AS-5646S, Research & Diagnostic Antibodies, Las Vegas, NV, USA) followed by FITC conjugated secondary antibody (donkey anti rabbit-FITC, sc-2090, Santa Cruz Biotechnology, Dallas TX, USA). Polymerized actin was stained with ActinGreenTM 488 (Molecular Probes, Eugene OR, USA) during secondary antibody incubation. Nuclei were stained after antibody incubation using NucBlue® (4′,6-diamidino-2-phenylindole or DAPI, Molecular Probes, Eugene OR, USA) for 5 minutes during the first of three PBS rinses. Samples were mounted using ProLong® Diamond Antifade Mountant (Molecular Probes, Eugene OR, USA). For some experiments, transient transfection with a calcineurin activity reporter containing eYFP and CFP driven by the human synapsin promotor was used to observe neuronal morphology (kindly donated by Dr. Charles Hoeffer, Institute for Behavioral Genetics, University of Colorado, Boulder, USA). Images were obtained with a confocal microscope (Nikon A1R, BioFrontiers Advanced Light Microscopy Core, University of Colorado, Boulder).

2.10. Data calculations

Total, intracellular and plasma membrane specific [^{125}I]epibatidine binding was compared for primary neuronal cultures from all brain regions by a two-way ANOVA with Tukey post-hoc analysis including nicotine concentration and α4 isoform as the variables. Cluster analysis was done using ICY imaging software (Copyright 2011 Institut Pasteur). Active contour plugin was used to obtain clusters signal intensity, area and the ratio of both to represent density of the signal. Two-way ANOVA with Sidak's post-hoc analysis was used to compare cluster parameters among α4 isoforms. SigmaPlot 12.0 was used to obtain K_d and B_{max} values. Prism Graph pad was used for statistical calculations and graphical presentation of the data.

3. Results

3. 1. Characterization of re-expression of α4 WT and S336A, S470A and S530A mutations.

Previously, we demonstrated that 97% of [^{125}I]epibatidine binding sites are eliminated by cytisine inhibition in neurons prepared from hippocampal and diencephalon cultures [8].

However, the percentage of α4 dependent [^{125}I]epibatidine binding sites in subcortical cultures has not been characterized. Therefore, [^{125}I] epibatidine binding was assessed in subcortical neurons prepared form α4 KO mice. Results indicated that 15 % of [^{125}I]epibatidine binding sites in subcortical cultures are non-α4β2*. However, these remaining sites were found to be insensitive to chronic nicotine treatment in terms of upregulation in total, intracellular and surface binding (Figure 1). After assessing the non-α4 binding component in subcortical neurons, AAV2 vectors containing WT and mutated α4 nAChR subunits were used to infect α4 KO neurons and re-express α4β2* nAChRs. To establish whether the mutant α4 subunits altered basic binding parameters, saturation binding assays were performed to determine dissociation constants (K_d) and maximal binding (Figure 2A). Results indicated that there were no significant differences in K_d among groups (Figure 2B, one-way ANOVA, ($F_{(3, 20)} = 2.931$, N=5). Although there was a trend for a reduced B_{max} for the S336A mutant, B_{max} values also did not significantly differ among the α4 isoforms (Figure 2C, one-way ANOVA, $F_{(3, 20)} = 1.829$, N=5). Basal levels of total [^{125}I]epibatidine binding sites in neurons infected with WT and mutant α4 AAVs were then compared among neuronal cultures prepared from the three brain regions. Total, intracellular and surface [^{125}I]epibatidine binding sites were similar between cortex and hippocampus, however, subcortical neurons expressed more total [^{125}I]epibatidine binding sites (Figure 2D, two-way ANOVA, brain region factor, $F_{(2, 82)} = 22.95$, $P < 0.0001$). The higher level of [^{125}I] epibatidine binding sites in subcortical neurons is likely due to the non-α4β2* nAChRs in this region that can be detected with this assay (see figure 1). When intracellular and surface binding sites in the three brain regions were compared, binding sites at intracellular membranes in subcortical neurons displayed a higher relative expression compared to cortical neurons (Figure 2E, two-way ANOVA, brain region factor $F_{(2, 85)} = 19.64$, $P < 0.0001$). Surface binding sites were not different among groups (Figure 2F). Net amount of total binding sites obtained with AAV infection were higher for cortex (37.44 ± 4.1 fmol/mg) and hippocampus (49.2 ± 8.5 fmol/mg) but similar for subcortex (68.54 ± 4.7 fmol/mg) compared to primary neurons prepared from WT C57BL/6 mouse embryos expression (cortex: 13.0 ± 0.9; hippocampus: 8.6 ± 0.7; diencephalon: 31.1 ± 2.4 and midbrain/hindbrain 97.4 ± 11.5 that in this study were combined into subcortex). Nonetheless, [^{125}I]epibatidine sites obtained with AAV infection in the present study are similar to those found in adult mouse brain [13].

3.2. Effect of serine mutations on α4β2* nAChR upregulation.

The effect of chronic nicotine treatment on total, intracellular and surface [^{125}I]epibatidine binding sites was measured in α4KO neuronal cultures after infection with WT and mutated α4 subunits. A concentration dependent increase in total specific [^{125}I]epibatidine binding sites was observed in all brain regions (Figure 3 upper panel, two-way ANOVA drug factor, Hp: $F_{(3, 87)} = 40.63$ $P < 0.0001$, Cx: $F_{(3, 112)} = 107.4$ $P < 0.0001$, SCx: $F_{(3, 132)} = 35.81$ $P < 0.0001$). No main effect of mutation or interaction of drug by mutation was detected for total binding. However, after a multiple comparison test a significant difference between WT and S336A mutation was observed at 10 μM nicotine in subcortical neurons (Figure 3 upper right panel, $p<0.05$). A main effect of nicotine treatment also was observed for intracellular [^{125}I]epibatidine binding (Figure 3 middle panel, two-way ANOVA drug factor, Hp: $F_{(3, 84)} = 70.81$ $P < 0.0001$, Cx: $F_{(3, 96)} = 17.77$ $P < 0.0001$, SCx: $F_{(3, 123)} = 39.36$ $P < 0.0001$).

Similar to total binding, there was no interaction of drug by mutation for intracellular binding, however, a main effect of mutation was detected (two-way ANOVA, $F_{(3, 84)} = 3.063$ $P = 0.0325$). A significant difference was observed in hippocampal intracellular binding between neurons expressing the S470A mutation compared with WT at 1 μM nicotine (Figure 3B, $p<0.05$ Tukey post-hoc test).

For cell surface binding, a main effect of nicotine treatment was found for all brain regions (Figure 3 lower panel, two-way ANOVA, Hp: $F_{(3, 75)} = 10.80$ $P < 0.0001$, Cx: $F_{(3, 96)} = 20.59$ $P < 0.0001$, SCx: $F_{(3, 123)} = 3.559$ $P = 0.0163$). A main effect of mutation on surface binding was also observed for hippocampus and subcortex but not for cortex (Figure 3 lower panel, two-way ANOVA mutation factor, Hp: $F_{(3, 75)} = 3.562$ $P = 0.0181$, SCx: $F_{(3, 123)} = 4.502$ $P = 0.0049$). The interaction between treatment and mutation was not significant. Upregulation of surface [^{125}I]epibatidine binding triggered by chronic nicotine treatment was affected by the three serine mutations, however different brain regions displayed different responses to the serine mutations. While none of the mutations affected surface upregulation in cerebral cortical neurons, the S336A mutation failed to exhibit surface upregulation in hippocampal or subcortical neurons at any nicotine concentrations tested (Figure 3C lower panels, $p<0.05$). Similarly, there was less surface binding in S470A relative to WT at 1 μM nicotine in hippocampus and both 1 μM and 10 μM in subcortex. The S530 mutant exhibited reduced surface upregulation at 1 μM in subcortex and a trend towards reduced upregulation at 10 μM in hippocampus.

3.3. Characterization of surface α4β2* nAChR clusters

Surface α4β2* nAChR were detected by labeling both α4 (mAb299) and β2 (AS-5646S) subunits in primary hippocampal neurons prepared from WT C57BL/6 embryos. A consistent co-localization of α4 subunits (red) with β2 subunits (green) was observed (Figure 4A). A higher magnification view of surface α4β2* nAChR shows formations or clusters in the neuronal soma (Figure 4B). A three-dimensional analysis of the image in figure 4B displays the superficial distribution of the labeling as indicated by the right insert where left represents the bottom of the z-stack and right the top, or in the bottom insert where up represents the bottom of the neuron and lower end represents the surface of the neuron (Figure 4C). This analysis confirmed the surface expression of the α4 clusters. No surface labeling with the anti α4-subunit antibody was observed in hippocampal neurons prepared from β2-nAChR KO mouse embryos demonstrating the necessity of β2 for trafficking of α4 nAChRs to the cell surface (Figure 4D).

Surface α4β2* nAChR labeling was also measured in α4 KO hippocampal neurons infected with AAV vector containing the WT α4 subunit. Consistent to what was observed with native α4* nAChRs, the re-expressed α4 WT subunit exhibited domains with intense α4 labeling (detected with anti-HA antibody) in the neuron soma and neurites (figure 4E). A higher magnification image is shown in a hippocampal neuron expressing surface α4(HA)β2* nAChR and YFP (Figure 4F). No HA staining was detected for non-infected α4KO neurons confirming the specificity of the HA antibody to detect HA-tagged α4 subunits. Permeabilization of WT α4 infected neurons to detect intracellular α4 expression

indicated that there is a homogeneous distribution of α4 subunits in α4 KO neurons infected with WT α4 AAV (Figure 4H).

To determine if α4β2* nAChR clusters also form in vivo,the wild-type α4-nAChR subunit was re-introduced in the dorsal hippocampus of α4 KO mice by intracranial injection of α4-AAV virus. Hippocampus was selected for re-expression of α4β2* nAChRs since the in vitro cluster analyses were done in primary hippocampal neurons. Similar to the in vitro results, dense clusters of α4β2* nAChR were found in the site of injection (CA1 region of the hippocampus, figure 5 C, D) and in neurons at the entorhinal cortex (Figure 5 A, B) indicating retrograde transport of AAV2 in performant path projection neurons [24].

3.4. Effect of nicotine treatment and serine mutations on α4β2* clusters

To determine the effect of nicotine treatment and the α4 mutations on the surface clusters of α4β2 nAChRs, hippocampal neurons isolated from α4 KO mice were infected with WT and the mutant forms of α4 and subsequently treated with vehicle or 1 μM nicotine for 48 hr. Following treatment, two parameters of the clusters were examined: signal intensity, a measure of the intensity of anti-HA staining (i.e, α4β2* nAChRs) per cluster and the average surface area per cluster. For signal intensity, there was a main effect of mutation ($F_{(3, 327)} = 9.349$, $p < 0.0001$) and a significant interaction of drug versus mutation ($F_{(3, 327)} = 8.64$, $p < 0.0001$). For the WT α4 and S336A mutant, nicotine increased the signal intensity of the cluster while there was no effect of nicotine treatment on the signal intensity for the S470A mutant. A trend for decreased intensity for the S530A mutant. The area of the α4β2* nAChR clusters (137.2 μm^2 in average for WT α4β2* nAChR) was affected by treatment ($F_{(1, 337)} = 9.483$, $p < 0.005$) and had a significant treatment by mutation interaction ($F_{(3,337)} = 5.397$, $p < 0.005$). Overall, the S336A mutant exhibited increased cluster area in response to nicotine treatment while the cluster area of the other α4 isoforms was unaffected by nicotine. Density of α4β2* expression in the clusters was also analyzed by dividing signal intensity by the area (Figure 6C). A significant main effect of mutation ($F_{(3,329)} = 9.27$, $p < 0.0001$) and an interaction between drug treatment and mutation was found ($F_{(3, 329)} = 12.83$, $p < 0.0001$). The density of WT α4β2* nAChRs clusters had a trend to increase but was not significantly affected by nicotine. The S336A mutant displayed an increase in cluster density (Figure 6C, $p<0.05$, Sidak's post hoc test). No change in cluster density was detected for the S470A mutant but in contrast, nicotine treatment significantly reduced the density of α4β2* nAChRs in the clusters for the S530A mutation (Figure 6C, $P<0.05$, Sidak's post hoc test).

4. Discussion

In this study, we examined the role of three serine residues in the MIII-MIV intracellular loop of the α4 nAChR subunit on basal expression and nicotine-induced upregulation of α4β2* receptors in neurons. We found that neurons that express α4 nAChR subunits containing serine to alanine mutations in positions S336, S470 and to some extent S530 failed to upregulate α4β2* receptors in the plasma membrane after chronic nicotine exposure. Neurons from all three brain regions exhibited similar levels of nicotine-induced upregulation of total α4β2* nAChR binding sites and other than an effect of the S336A

mutant on total binding sites in subcortex at 10 μM nicotine, the mutants also had little impact on total binding sites. Interestingly, the ability of the mutant α4 subunits to impair upregulation of plasma membrane α4β2* nAChRs was brain region specific; surface upregulation was reduced in hippocampus and subcortex but not cortex. Previous studies have shown that upregulation of total α4β2* nAChR binding sites *in vivo* is brain region specific [2,13–16]. Adding further to the complexity of upregulation, the current study demonstrates that even among brain regions where upregulation of total binding sites occurs there may be multiple, potentially neuron-type specific, mechanisms that contribute to nicotine upregulation-induced surface α4β2* expression.

In contrast to our findings, Fenster et al. [25] reported that the S336A mutant enhanced rather than reduced surface expression of α4β2 in response to nicotine exposure. The reason for the discrepancy between our results and the results of Fenster et al. is not known. However, there are several plausible explanations. A few possibilities include the different cell types used and the method for expressing α4β2 nAChRs. Fenster heterologous expressed α4β2 nAChRs in frog oocytes while we re-expressed α4β2* nAChRs in neurons that natively express α4β2* nAChRs. It is likely that the cellular machinery involved in nAChR trafficking and upregulation differ between these cell types. Further, neurons express other nAChR subunits that may impact upregulation. For example, α4β2* nAChRs that include an α5 subunit do not upregulate [26]. Therefore, caution should be taken when interpreting results from a single cell type. Although no previous studies have examined the role of S470 on nicotine-induced upregulation, Jeanclos et al. [19] reported that this residue is important for cell surface expression of α4β2 nAChRs. This group found that the S470A mutation, when heterologously expressed with β2 in HEK ts293 cells, exhibited reduced basal surface expression of α4β2 nAChRs relative to wild type α4. In contrast, we found that this mutation affected surface expression of α4β2* nAChRs following continuous nicotine exposure but did not affect basal surface expression in any of the neuronal populations examined. The absence of an effect of Serine mutations on basal nAChR expression suggests that protein domains within nAChR associated to basal expression may differ from those that control upregulation.

The observation that the findings from primary neurons differ from the results of heterologous expression systems, again, suggests caution should be taken when interpreting results from a single cell type. Although heterologous systems such as oocytes and HEK cells have and continue to be a very useful method for assessing nAChR function, they do not express nAChRs natively and likely possess different cellular machinery for assembly and trafficking of nAChRs. This is exemplified by the fact that these heterologous systems do not express proteins known to be involved in in vivo nAChR trafficking including Ric3 [27], VILIP-1 [28,29], and Nacho [30] among others. In contrast, primary neurons provide a more physiologically relevant in vitro system for studying nAChRs since they naturally express nAChRs and thus possess neuron-relevant cellular machinery involved in regulating the assembly, trafficking and expression of nAChRs. Nonetheless, the ultimate test will be to determine the impact of the serine mutants on upregulation in vivo.

An intriguing finding of the current study is that although the α4 mutants affected surface upregulation of α4β2* nAChRs, they did not alter the upregulation of total α4β2*nAChRs.

Considerable evidence has accumulated that indicates that nicotine acts intracellularly as a molecular chaperone to increase the efficiency of assembly and stability of α4β2* nAChRs in the endoplasmic reticulum [31]. This chaperone effect of nicotine likely underlies the observed upregulation of total α4β2* nAChRs independent of α4 isoform. However, the fact that mutations in α4 don't affect upregulation of total receptors but do prevent surface upregulation indicate that the mutations likely impact surface upregulation at a stage following the chaperone effect of nicotine. What this mechanism might be is not known. Henderson et. al (2014) reported that nicotine induces rapid assembly of immature nAChRs in the ER. However, in order for these immature receptors to be trafficked to the surface, retrograde transport from the cis-Golgi to the ER must occur for proper receptor maturation. Perhaps the serine mutants in this study are necessary for this retrograde transport. This interpretation would be consistent with the finding that a mutation in the β3 nAChR subunit that affects retrograde trafficking from the cis-Golgi to ER affects functional upregulation but does not alter normal expression [32]

S336, S470 and possibly S530 may also impact surface binding through altering the trafficking of the upregulated receptors to the cell surface, perhaps through interaction with protein chaperones like 14–3-3η which is known to interact with S470 [19] or by stabilization of surface α4β2* nAChRs through interaction with proteins such as VILIP-1 which interacts with a region of the α4 subunit that includes S336 [29]. It also has been established that upregulation of α4β2* nAChRs is dependent upon stoichiometry [33]. α4β2* nAChRs with a stoichiometry of $(\alpha4)_2(\beta2)_3$ upregulate whereas those with an $(\alpha4)_3(\beta2)_2$ stoichiometry or an $(\alpha4)_2(\beta2)_2(\alpha5)$ composition do not upregulate. Therefore, another plausible mechanism through which the mutations might affect upregulation is though altering receptor stoichiometry. The brain region selectivity of the mutations on upregulation could therefore be a consequence of region-specific availability of other nAChR subunits. Future studies to explore the specific roles of these α4 serine residues in upregulation, including potential alterations in receptor stoichiometry may provide new insight into the cell type dependent mechanisms of α4β2* nAChR upregulation. We speculate that nAChR upregulation is not a homogeneous response among brain regions due to a specific array of neuronal types and possibly a differential expression of proteins that control nAChR upregulation in every cell type. As an example, the chaperone protein RIC-3 has two major isoforms that have different expression across the brain and those isoforms differentially regulate nAChR expression [34].

Another novel finding of the current study was the discovery that α4β2* nAChRs form clusters on the plasma membrane of neurons. The existence of nicotinic receptor clusters in the postsynaptic region of the neuromuscular junction has been well documented for muscle type nAChR [35,36]. However, the data described in the current study are the first, to our knowledge, to report that α4β2* nAChRs form clusters in the plasma membrane. Clusters of α4β2* nAChRs were often observed at the soma of neurons and somewhat less frequently at neuronal processes (Figure 4). The formation of plasma membrane α4β2* nAChR clusters was confirmed when WT α4 and the three mutant forms of α4 were re-expressed in neurons derived from α4 KO mice. The absence of α4 nAChR subunit expression in the plasma membrane of β2 KO neurons (Figure 4) is consistent with previous reports that demonstrate

the interdependence of α4 and β2 nAChR subunit expression [37] and confirm that the α4 nAChR being assessed in the experiments is α4β2*.

Moreover, clusters of α4β2* nAChR were found in mouse brain when AAV particles containing α4-HA was injected in the CA1 region of the hippocampus. Those receptor clusters were also found at the medial entorhinal cortex (Figure 5), observing the trafficking of nAChR through the performant pathway. This result indicates that the clusters are not an artifact that occur only in cultured neurons.

Although the cluster data for the mutants do not appear to be consistent with the binding data, it is important to note that all cluster analyses were performed on α4β2* nAChRs expressed on the cell soma and proximal dendrites. This comprises a very minor fraction of the total neuronal surface. Further, it is not technically feasible to determine the total number of clusters per neuron. Without quantification of all clusters for a given neuron, it is not meaningful to attempt to compare the binding data, which represents all receptors per neuron, with the cluster data. Regardless, the discovery of α4β2* clusters indicates that there may be another aspect of nicotine treatment on the cellular distribution of α4β2* nAChR that needs to be carefully considered.

Since serine is an amino acid that can be phosphorylated, it is possible that the effect of the serine to alanine mutations reported here are due to a loss of phosphorylation of the examined residues. However, of the serine residues in the present study, direct phosphorylation has only been demonstrated for S470 by PKA in frog oocytes [38]. Therefore, whether the effect of the mutations on surface upregulation and plasma membrane clusters is due to the loss of receptor phosphorylation or an alternative mechanism remains to be determined.

The consequences of α4β2* nAChR upregulation in smokers is unknown. However, upregulation of α4β2* nAChRs in hippocampus has been implicated in nicotine withdrawal-induced learning deficits in mice. Gould et al. [39] reported that the duration of withdrawal-induced learning deficits, as measured using contextual fear conditioning, paralleled changes in α4β2* nAChRs. However, the relationship between withdrawal-induced learning deficits and hippocampal α4β2* nAChR levels was correlational, and therefore, a causal relationship cannot be established. Further, α4β2* levels were determined using whole homogenate ligand binding, so it is not known if the level of surface α4β2* nAChRs also paralleled the recovery of learning in the animals. Understanding the role of upregulation in nicotine withdrawal-induced cognitive impairment is of considerable importance since it is a common symptom of smoking cessation and is a strong predictor of relapse [40]. The introduction of e-cigarettes and the increase in popularity of hookah use increases the urge for nicotine dependence therapies, considering that those nicotine devices can deliver similar or even higher plasma nicotine concentrations than regular cigarettes [41,42]. Perhaps studies with rodents expressing α4 mutants like S336 that don’t surface upregulate in the hippocampus may provide important insight into the role of surface upregulation in this and potentially other important withdrawal symptoms.

In conclusion, serine residues in the MIII-MIV intracellular loop of the α4 nAChR subunit have a brain region dependent modulatory role on surface α4β2* nAChR upregulation that appears to be independent of total α4β2* upregulation. Further studies with these mutants may provide insight into the cellular and molecular mechanisms of upregulation as well as improve our understanding of the role of α4β2*upregulation on behaviors relevant to nicotine dependence.

Acknowledgments

This work was supported by NIH-NIDA DA036673.

5. References

[1]. Wu J, Lukas RJ, Naturally-expressed nicotinic acetylcholine receptor subtypes, Biochem. Pharmacol 82 (2011) 800–807. [PubMed: 21787755]

[2]. Marks MJ, Burch JB, Collins AC, Effects of chronic nicotine infusion on tolerance development and nicotinic receptors, J. Pharmacol. Exp. Ther 226 (1983) 817–25. [PubMed: 6887012]

[3]. Schwartz RD, Kellar KJ, Nicotinic cholinergic receptor binding sites in the brain: regulation in vivo, Science 220 (1983) 214–6. [PubMed: 6828889]

[4]. Benwell ME, Balfour DJ, Anderson JM, Evidence that tobacco smoking increases the density of (−)-[3H]nicotine binding sites in human brain, J. Neurochem 50 (1988) 1243–7. [PubMed: 3346676]

[5]. Breese CR, Marks MJ, Logel J, Adams CE, Sullivan B, Collins AC, Leonard S, Effect of smoking history on [^{3}H]nicotine binding in human postmortem brain, J. Pharmacol. Exp. Ther 282 (1997) 7–13. [PubMed: 9223534]

[6]. Perry DC, Dávila-García MI, Stockmeier CA, Kellar KJ, Increased nicotinic receptors in brains from smokers: membrane binding and autoradiography studies, J. Pharmacol. Exp. Ther 289 (1999) 1545–52. [PubMed: 10336551]

[7]. Lomazzo E, Hussmann GP, Wolfe BB, Yasuda RP, Perry DC, Kellar KJ, Effects of chronic nicotine on heteromeric neuronal nicotinic receptors in rat primary cultured neurons, J. Neurochem 119 (2011) 153–64. [PubMed: 21806615]

[8]. Zambrano CA, Salamander RM, Collins AC, Grady SR, Marks MJ, Regulation of the Distribution and Function of [^{125}I]Epibatidine Binding Sites by Chronic Nicotine in Mouse Embryonic Neuronal Cultures, J. Pharmacol. Exp. Ther 342 (2012) 245–254. [PubMed: 22532626]

[9]. Peng X, Gerzanich V, Anand R, Whiting PJ, Lindstrom J, Nicotine-induced increase in neuronal nicotinic receptors results from a decrease in the rate of receptor turnover, Mol. Pharmacol 46 (1994) 523–30. [PubMed: 7935334]

[10]. Govind AP, Walsh H, Green WN, Nicotine-induced upregulation of native neuronal nicotinic receptors is caused by multiple mechanisms, J. Neurosci 32 (2012) 2227–38. [PubMed: 22323734]

[11]. Kuryatov A, Luo J, Cooper J, Lindstrom J, Nicotine acts as a pharmacological chaperone to up-regulate human alpha4beta2 acetylcholine receptors, Mol. Pharmacol 68 (2005) 1839–51. [PubMed: 16183856]

[12]. Fenster CP, Beckman ML, Parker JC, Sheffield EB, Whitworth TL, Quick MW, Lester RA, Regulation of alpha4beta2 nicotinic receptor desensitization by calcium and protein kinase C, Mol. Pharmacol 55 (1999) 432–43. [PubMed: 10051526]

[13]. Marks MJ, Rowell PP, Cao J-Z, Grady SR, McCallum SE, Collins AC, Subsets of acetylcholine-stimulated $^{86}Rb^{+}$ efflux and [^{125}I]-epibatidine binding sites in C57BL/6 mouse brain are differentially affected by chronic nicotine treatment, Neuropharmacology 46 (2004) 1141–1157. [PubMed: 15111021]

[14]. Flores CM, Dávila-García MI, Ulrich YM, Kellar KJ, Differential regulation of neuronal nicotinic receptor binding sites following chronic nicotine administration, J. Neurochem 69 (1997) 2216–9. [PubMed: 9349569]

[15]. Sanderson EM, Drasdo AL, McCrea K, Wonnacott S, Upregulation of nicotinic receptors following continuous infusion of nicotine is brain-region-specific, Brain Res 617 (1993) 349–52. [PubMed: 8402163]

[16]. Nguyen HN, Rasmussen BA, Perry DC, Subtype-Selective Up-Regulation by Chronic Nicotine of High-Affinity Nicotinic Receptors in Rat Brain Demonstrated by Receptor Autoradiography, J. Pharmacol. Exp. Ther 307 (3) (2003) 1090–7. [PubMed: 14560040]

[17]. Kracun S, Harkness PC, Gibb AJ, Millar NS, Influence of the M3-M4 intracellular domain upon nicotinic acetylcholine receptor assembly, targeting and function, Br. J. Pharmacol 153 (2008) 1474–1484. [PubMed: 18204482]

[18]. López-Hernández GY, Biaggi-Labiosa NM, Torres-Cintrón A, Ortiz-Acevedo A, Lasalde-Dominicci JA, Contribution of Position α4S336 on Functional Expression and Up-regulation of α4β2 Neuronal Nicotinic Receptors, Cell. Mol. Neurobiol 29 (2009) 41–53. [PubMed: 18818999]

[19]. Jeanclos EM, Lin L, Treuil MW, Rao J, DeCoster MA, Anand R, The Chaperone Protein 14–3-3η Interacts with the Nicotinic Acetylcholine Receptor α4 Subunit, J. Biol. Chem 276 (2001) 28281–28290. [PubMed: 11352901]

[20]. Bermudez I, Moroni M, Phosphorylation and Function of α4β2 Receptor, J. Mol. Neurosci 30 (2006) 97–98. [PubMed: 17192645]

[21]. Pollock VV, Pastoor TE, Wecker L, Cyclic AMP-dependent protein kinase (PKA) phosphorylates Ser362 and 467 and protein kinase C phosphorylates Ser550 within the M3/M4 cytoplasmic domain of human nicotinic receptor alpha4 subunits, J. Neurochem 103 (2007) 456–66. [PubMed: 17897355]

[22]. Zambrano CA, Short CA, Salamander RM, Grady SR, Marks MJ, Density of α4β2* nAChR on the surface of neurons is modulated by chronic antagonist exposure, Pharmacol. Res. Perspect 3 (2015) e00111. [PubMed: 25729578]

[23]. Dávila-García MI, Houghtling RA, Qasba SS, Kellar KJ, Nicotinic receptor binding sites in rat primary neuronal cells in culture: characterization and their regulation by chronic nicotine, Mol. Brain Res 66 (1999) 14–23. [PubMed: 10095073]

[24]. Kaspar BK, Erickson D, Schaffer D, Hinh L, Gage FH, Peterson DA, Targeted Retrograde Gene Delivery for Neuronal Protection, Mol. Ther 5 (2002) 50–56. [PubMed: 11786045]

[25]. Fenster CP, Whitworth TL, Sheffield EB, Quick MW, Lester RA, Upregulation of surface alpha4beta2 nicotinic receptors is initiated by receptor desensitization after chronic exposure to nicotine, J. Neurosci 19 (1999) 4804–14. [PubMed: 10366615]

[26]. Mao D, Perry DC, Yasuda RP, Wolfe BB, Kellar KJ, The α4β2α5 nicotinic cholinergic receptor in rat brain is resistant to up-regulation by nicotine in vivo, J. Neurochem 104 (2) (2008) 446–56. [PubMed: 17961152]

[27]. Lansdell SJ, Gee VJ, Harkness PC, Doward AI, Baker ER, Gibb AJ, Millar NS, RIC-3 Enhances Functional Expression of Multiple Nicotinic Acetylcholine Receptor Subtypes in Mammalian Cells, Mol. Pharmacol 68 (2005) 1431–1438. [PubMed: 16120769]

[28]. Lin L, Jeanclos EM, Treuil M, Braunewell K-H, Gundelfinger ED, Anand R, The calcium sensor protein visinin-like protein-1 modulates the surface expression and agonist sensitivity of the alpha 4beta 2 nicotinic acetylcholine receptor, J. Biol. Chem 277 (2002) 41872–8. [PubMed: 12202488]

[29]. Zhao C, Noack C, Brackmann M, Gloveli T, Maelicke A, Heinemann U, Anand R, Braunewell KH, Neuronal Ca^{2+} sensor VILIP-1 leads to the upregulation of functional α4β2 nicotinic acetylcholine receptors in hippocampal neurons, Mol. Cell. Neurosci 40 (2009) 280–292. [PubMed: 19063970]

[30]. Matta JA, Gu S, Davini WB, Lord B, Siuda ER, Harrington AW, Bredt DS, NACHO Mediates Nicotinic Acetylcholine Receptor Function throughout the Brain, Cell Rep 19 (2017) 688–696. [PubMed: 28445721]

[31]. Henderson BJ, Lester HA, Inside-out neuropharmacology of nicotinic drugs, Neuropharmacology 96 (2015) 178–93. [PubMed: 25660637]

[32]. Henderson BJ, Srinivasan R, Nichols WA, Dilworth CN, Gutierrez DF, Mackey EDW, McKinney S, Drenan RM, Richards CI, Lester HA, Nicotine exploits a COPI-mediated process for

chaperone-mediated up-regulation of its receptors, J. Gen. Physiol 143 (2014) 51–66. [PubMed: 24378908]

[33]. Moroni M, Zwart R, Sher E, Cassels BK, Bermudez I, 4beta2 Nicotinic Receptors with High and Low Acetylcholine Sensitivity: Pharmacology, Stoichiometry, and Sensitivity to Long-Term Exposure to Nicotine, Mol. Pharmacol 70 (2006) 755–768. [PubMed: 16720757]

[34]. Ben-David Y, Mizrachi T, Kagan S, Krisher T, Cohen E, Brenner T, Treinin M, RIC-3 expression and splicing regulate nAChR functional expression, Mol. Brain 9 (2016) 47. [PubMed: 27129882]

[35]. Ramarao MK, Cohen JB, Mechanism of nicotinic acetylcholine receptor cluster formation by rapsyn, Proc. Natl. Acad. Sci. U. S. A 95 (1998) 4007–12. [PubMed: 9520483]

[36]. Wu H, Xiong WC, Mei L, To build a synapse: signaling pathways in neuromuscular junction assembly, Development 137 (2010) 1017–33. [PubMed: 20215342]

[37]. Whiteaker P, Cooper JF, Salminen O, Marks MJ, Mcclure-Begley TD, Brown RWB, Collins AC, Lindstrom JM, Immunolabeling demonstrates the interdependence of mouse brain α4 and β2 nicotinic acetylcholine receptor subunit expression, J. Comp. Neurol 499 (2006) 1016–1038. [PubMed: 17072836]

[38]. Guo X, Wecker L, Identification of three cAMP-dependent protein kinase (PKA) phosphorylation sites within the major intracellular domain of neuronal nicotinic receptor alpha4 subunits, J. Neurochem 82 (2002) 439–47. [PubMed: 12124445]

[39]. Gould TJ, Portugal GS, André JM, Tadman MP, Marks MJ, Kenney JW, Yildirim E, Adoff M, The duration of nicotine withdrawal-associated deficits in contextual fear conditioning parallels changes in hippocampal high affinity nicotinic acetylcholine receptor upregulation, Neuropharmacology 62 (2012) 2118–2125. [PubMed: 22285742]

[40]. Rukstalis M, Jepson C, Patterson F, Lerman C, Increases in hyperactive-impulsive symptoms predict relapse among smokers in nicotine replacement therapy, J. Subst. Abuse Treat 28 (2005) 297–304. [PubMed: 15925263]

[41]. Shafagoj YA, Mohammed FI, Hadidi KA, Hubble-bubble (water pipe) smoking: levels of nicotine and cotinine in plasma, saliva and urine, Int. J. Clin. Pharmacol. Ther 40 (2002) 249–55. [PubMed: 12078938]

[42]. Hiler M, Breland A, Spindle T, Maloney S, Lipato T, Karaoghlanian N, Shihadeh A, Lopez A, Ramôa C, Eissenberg T, Electronic cigarette user plasma nicotine concentration, puff topography, heart rate, and subjective effects: Influence of liquid nicotine concentration and user experience, Exp. Clin. Psychopharmacol 25 (2017) 380–392. [PubMed: 29048187]

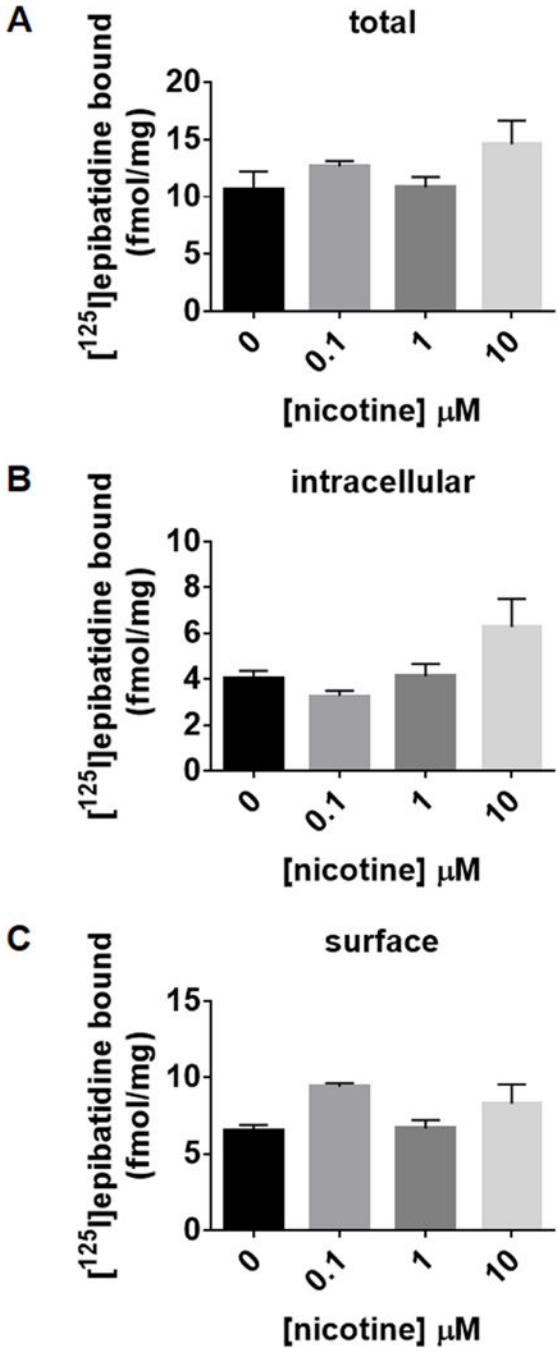

Figure 1: Expression of non-α4β2* nAChR high affinity [^{125}I]epibatidine binding sites.

Basal levels of total (A), intracellular (B) and surface (C) [^{125}I]epibatidine binding sites in subcortical neurons prepared from α4 KO mouse embryos. Neurons were challenged with 0, 0.1, 1 and 10 μM nicotine for 4 days. [^{125}I]epibatidine binding represents endogenous non-α4β2 nAChRs. Data represents mean ± S.E.M obtained from N= 3.

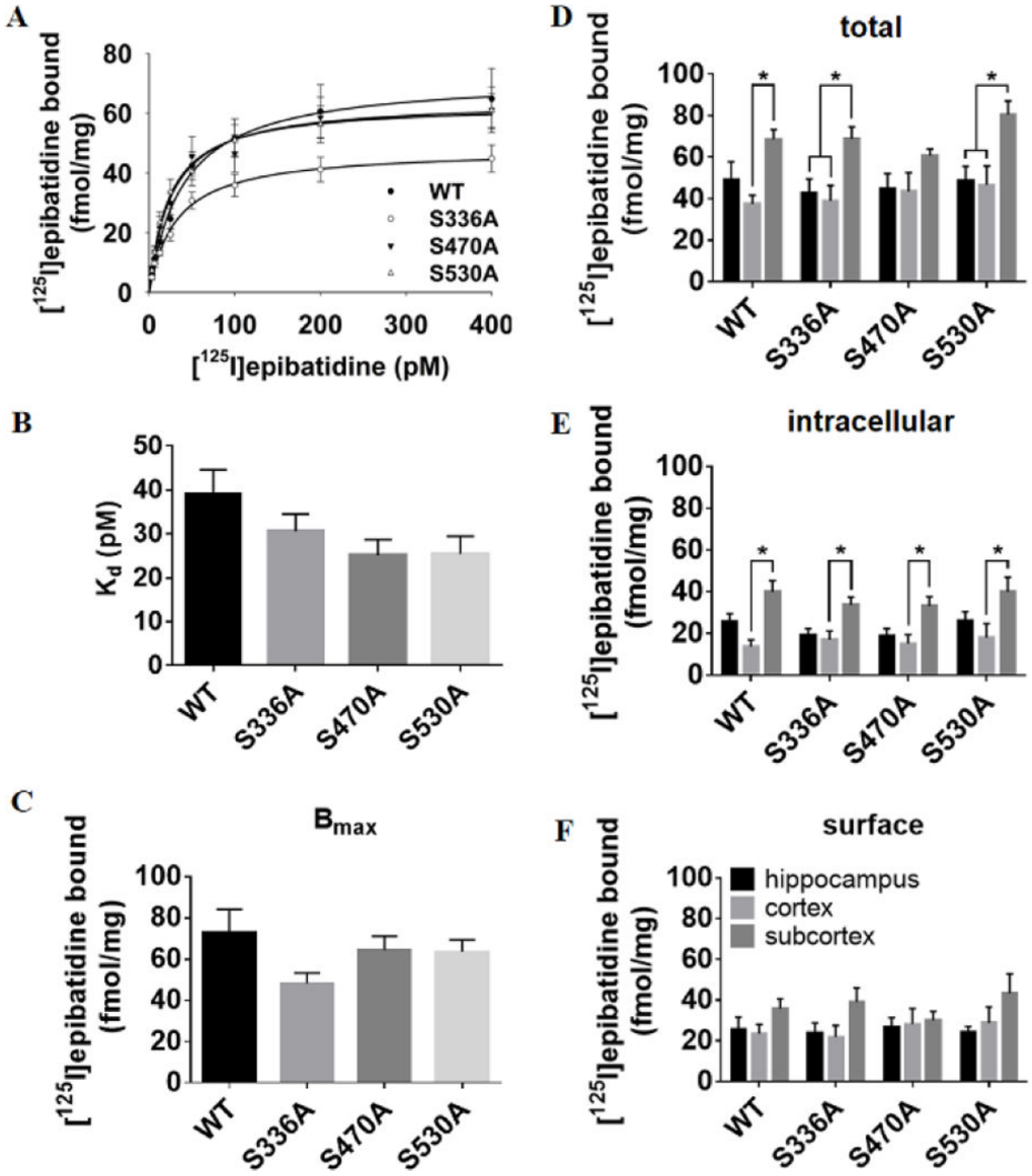

Figure 2: Preliminary characterization of expression model for α4HA subunits in α4 KO neurons.

(A) Saturation binding in hippocampal α4KO neurons infected with AAV containing WT and S336A, S470A and S530A mutant α4 subunits. Affinity constants (B) and maximal binding (C) is shown. Comparison of total (D), intracellular (E) and surface (F) [^{125}I]epibatidine binding sites in neuronal cultures prepared from the three brain regions after infection with similar AAV titers. Data was obtained from N=5 for B_{max} and K_d calculations and N=6, 8 and 10 for binding sites comparison in Hp, Cx and SCx respectively.

Data represented are mean ± S.E.M. Asterisks denote significant differences by a two-way ANOVA, Tukey post hoc test.

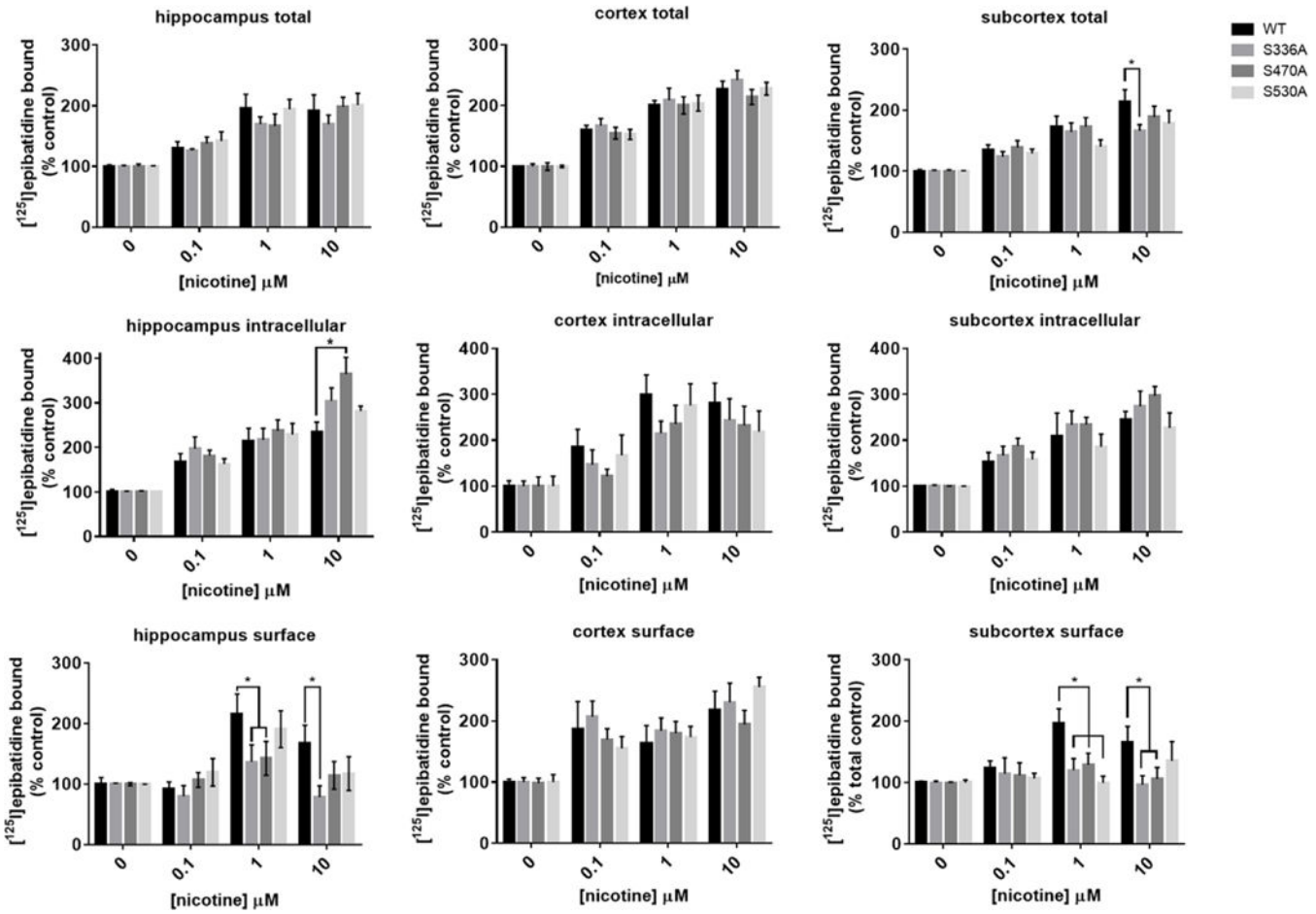

Figure 3: Nicotine dose-response study in α4KO neurons expressing α4-nAChR isoforms.

Neurons were challenged with 0, 0.1, 1 and 10 μM nicotine for 4 days. Represented are total (upper panels), intracellular (middle panels) and surface receptors in hippocampal (left panels) cortical (middle panels) and subcortical neurons (right panels). Total [^{125}I]epibatidine binding was normalized to control neurons (100%). Data obtained from N= 6, 8 and 10 replicates for Hp, Cx and SCx respectively. Data represented are mean ± S.E.M. Asterisks denote significant differences by a two-way ANOVA, Tukey post hoc test ($P<0.05$).

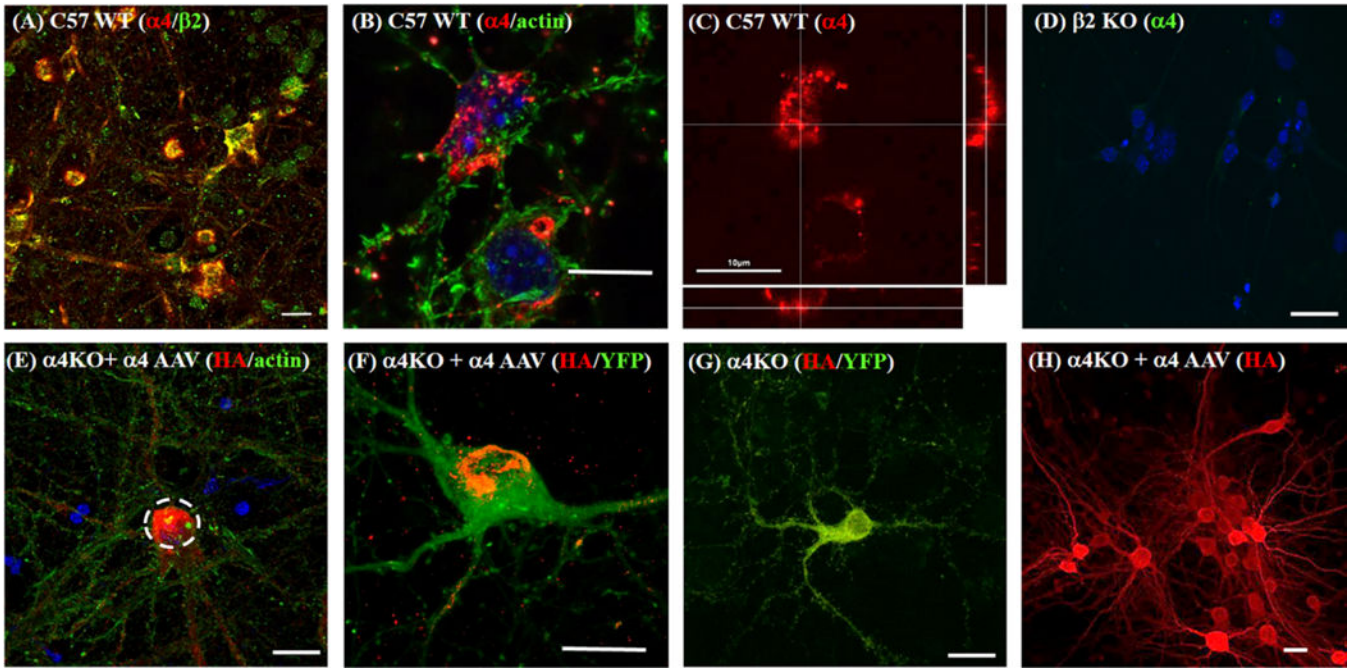

Figure 4: Surface immunolabeling of native and AAV infected α4 nAChR subunits in hippocampal neurons.

Native α4β2 nAChR expressed in the neuronal surface of hippocampal neurons (A-D). (A) Similar localization of both subunits is denoted by yellow co-staining of α4 (red) and β2 nAChR subunits (green). (B) High magnification (100X) of a hippocampal neuron stained with anti α4 antibody (red) phalloidin (green) and DAPI (blue) shows dense spots or clusters of nicotinic receptors. (C) Red channel extracted from figure 3B shows a 3D Z-stack reconstruction at the bottom for the horizontal coordinate and on the right for the vertical coordinate. (D) Hippocampal neuron prepared from a β2 KO mouse embryo displays DAPI nuclei staining (blue) but no green anti α4-FITC antibody staining in the neuronal surface. Re-expressed WT α4 nAChR subunit in α4 KO hippocampal neurons using AAVs (E-H). (E) Surface α4HA labeling (red surrounded by dashed line), polymerized actin (green) and nuclei (DAPI) is shown. (F) High magnification (100X) of a neuron expressing surface α4HA (red) and YFP (green) displays α4β2* nAChR clusters on the neuronal surface. (G) Control α4 KO neurons expressing YFP (green) not infected with WT α4 AAV displayed no surface labeling for α4HA (red). (H) Triton permeabilization exposed intracellular α4HA labeling (red). Scale bars represent 10 μm.

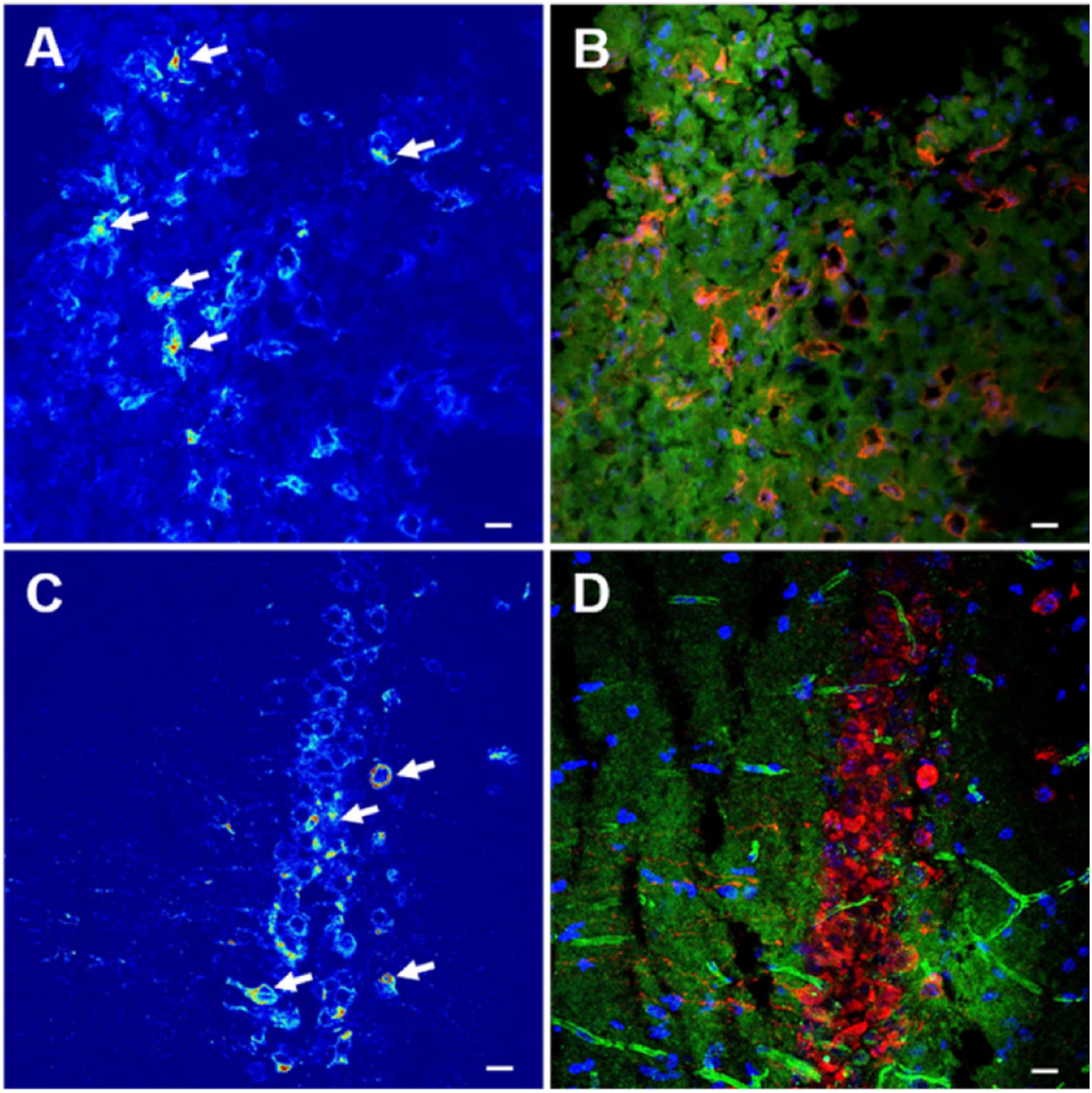

Figure 5: Detection of HA-tagged α4β2 nAChR clusters in mouse brain.

AAV containing α4-HA subunits were injected in CA1 hippocampal region. Mice were sacrificed 2 weeks after injections and brains were frozen. Coronal sections (14 μm) were fixed with paraformaldehyde and stained with anti-HA antibody. A and C represent HA labeling in pseudo color of a single 0.225 μm confocal section for medial entorhinal cortex and CA1 region, respectively. B and D represent the merged image of 45 confocal sections for A and C, respectively. Red, Green and Blue in B and D correspond to anti-HA,

phalloidin and DAPI staining, respectively. Arrows in A and C highlight the presence of dense clusters of α4β2* nAChR. Scale bars represent 10 μm.

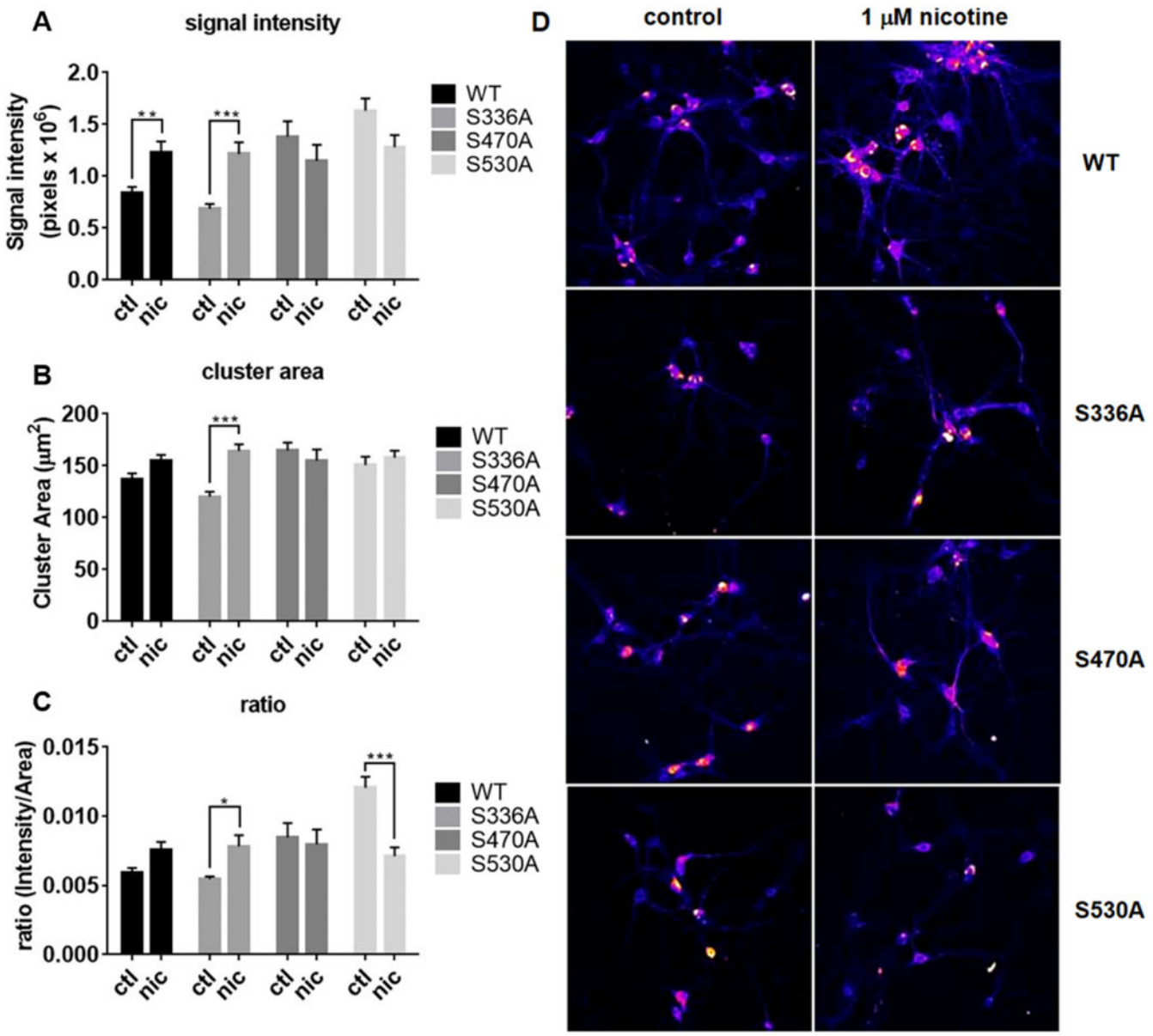

Figure 6: Analysis of surface α4β2* clusters for the different serine mutations in the α4 subunit.

(A) Sum intensity of the clusters obtained for α4 isoforms in control hippocampal neurons and chronically (4 days) 1 μM nicotine treated neurons. (B) Area or contour of the nAChR clusters is shown. (C) Density of the expression of α4β2* nAChR in those clusters is represented as sum intensity divided by the area of the cluster. (D) Representative pictures in pseudo color is shown for control neurons (left) and 1 μM nicotine treated neurons (right) and for WT α4 nAChR subunit (top panels) and the different serine mutations (lower panels). Data was obtained from 5 different preparations (N=5) in four independent preparations. Data represented are mean ± S.E.M. Asterisks represent significant differences obtained with a two-way ANOVA, Sidak's post hoc test (* $p<0.05$, ** $p<0.01$, *** $p<0.001$).